Substrate Cleaning using Ultrasonics/Megasonics

Mohammad Kazemi[1], Helmuth Treichel[2], Sharyl Maraviov[3], and Rito Ligutom[4]

[1]Contractor, San Jose, CA 95138, USA
[2]Sunsonix, 859 Pheland Ct, Milpitas, CA 95035, USA
[3]PCT Systems, Inc., 44060 Old Warm Springs Blvd., Fremont, CA. 94538, USA
[4]Contractor, Milpitas, CA 95035, USA

Corresponding Author: Helmuth Treichel, phone: +408.515.8585, e-mail: helmuth@sunsonix.com

1. Introduction

Driven by the shrinking feature-sizes in the semiconductor industry and a new awareness of particles in general compromising the performance of devices like photovoltaic cells, the size of the contaminating particles that need to be removed is pushed down. OEMs face increasingly stringent cleaning requirements. Failure to meet those requirements results in severe problems with yield and reliability. To this end, advanced cleaning techniques need to be developed to meet future cleaning challenges.

Ultrasonic/Megasonic cleaning (USC/MSC) appears to be promising in meeting the future demands for cleaning substrates [1]. Despite wide usages of USC/MSC, the underlying physics of particle dislodgement is not well understood [2]. Hence, the present paper focuses on exploring the physics of particle dislodgement subject to acoustic waves generated by piezoelectric transducers.

Van der Waals (VDW) force, ionic double layer force and hydrophobic force are the major forces of adhesion between a particle and a substrate (see Fig. 1). Those adhesion forces depend on particle diameter, hardness of particle and substrate, chemical composition of particle and substrate and the environment in which the contaminated substrate is located. Acoustic pressure (AP), acoustic streaming (AS) and acoustic cavitation (AC) are the detachment forces in USC/MSC system. Those detachment forces depend on particle diameter, transducer frequency, and power intensity of transducer and the chemical composition of the solution.

In this study, the adhesion and detachment forces of spherical particles with a diameter smaller than 400 nm are investigated. Two different cases are studied herein: a) glass particle and, b) alumina. Those cases correspond to practical substrate cleaning of glass and aluminum substrates, but can also be applied to silicon surfaces in general. The detachment of such particles subject to the acoustic waves generated by a piezoelectric transducer is investigated. For this purpose, two different transducer frequencies are studied, commonly used in USC/MSC tanks: 430 kHz and 950 kHz.
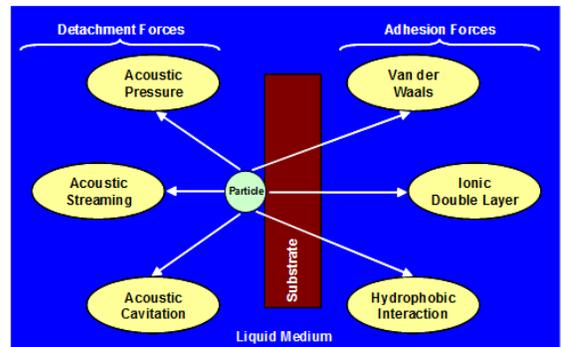

Fig. 1. Schematic of adhesion and detachment forces acting on a particle attached to a substrate in a liquid medium.

2. Particle Dislodgement Methods

A particle attached to a substrate can be dislodged if the detachment forces overcome the adhesion forces. With reference to Fig. 2, there are three methods through which a particle can be dislodged [3]:

- Rolling dislodgment
- Sliding dislodgment
- Lift-off dislodgment

Rolling dislodgment occurs when the detachment force creates a moment that exceeds the moment generated by the adhesion force. Under this circumstance, the particle rolls off and is detached from the substrate. The minimum detachment force required for rolling dislodgement can be calculated as follows:

$$F_{Det} \times (d/2 - b) \geq F_{Adh} \times a \qquad (1)$$

In this equation, F_{Det} and F_{Adh} are the resultant detachment and adhesion forces, respectively; d represents the particle diameter; a stands for the radius of contact and b is the particle penetration depth.
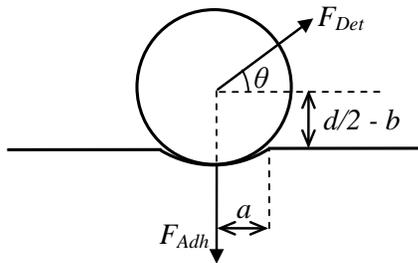

Fig. 2. Diagram of equivalent adhesion and detachment forces acting on a spherical particle that is attached to a substrate.

Sliding dislodgment occurs when the detachment force exceeds the coulomb friction force that is caused by the adhesion force. The minimum detachment force required for sliding dislodgement can be calculated as follows:

$$F_{Det} \geq \mu \, F_{Adh} \qquad (2)$$

In this equation, μ stands for the coulomb friction coefficient. The lift-off dislodgement occurs when the detachment force exceeds the adhesion force causing the particle to be directly pulled away from the substrate surface. The minimum detachment force required for lift-off dislodgement can be calculated as follows:

$$F_{Det} \geq F_{Adh} \qquad (3)$$

Among these dislodgment methods, rolling dislodgement is the most likely mechanism of dislodgement as it requires the lowest level of detachment force.

3. Adhesion Forces

There are three major types of the adhesion forces that a particle may experience in a liquid medium:

- Van der Waals (VDW) force
- Ionic double layer force
- Hydrophobic force

Van der Waals force is a short-range force that decays rapidly as the separation distance between the particle and substrate increases [4]:

$$F_{VDW} = \frac{A_{132}d}{12\,z_0^2} \qquad (4)$$

In this equation, A_{132} stands for the Hamaker constant between the particle (1) and substrate (2) in the medium (3) and z_0 represents the separation distance between the particle and substrate and is typically set to 0.4 nm for smooth surfaces. Table 1 summarizes the values of Hamaker between an alumina particle on an alumina substrate and a glass particle on a glass substrate in both air and water media. Inspection of data shown in table 1 reveals that: a) Hamaker constant in water is less than that in air; and, b) Hamaker constant for alumina-on-alumina is larger than that for glass-on-glass.

		in Air	in Water
A_{132}	Alumina-on-Alumina	1.400E-19	2.703E-20
	Glass-on-Glass	3.400E-20	6.437E-22

Table 1. Hamaker constants for e.g. alumina-on-alumina and e.g., glass-on-glass in both air and water media.

The VDW force between a particle and a substrate causes the deformation at the interface. The deformation increases the area of contact and consequently the VDW force which can be evaluated using the following equation [4]:

$$F_{VDW} = \frac{A_{132}d}{12\,z_0^2}\left[1+\frac{2a^2}{d\,z_0}\right] \qquad (5)$$

The radius of contact can be calculated using the JKR theory [5]:

$$a = \left[\frac{3\pi W_A d^2}{8\,E_{Comp}}\right]^{1/3} \qquad (6)$$

Where W_A represents the work of adhesion for an undeformed interface and E_{Comp} stands for the composite Young's modulus of elasticity at the interface. Work of adhesion and composite Young's modulus of elasticity can be calculated as follows [3,5,6]:

$$W_A = \frac{A_{132}}{12\pi\,z_0^2} \qquad (7)$$

$$E_{Comp} = \frac{4}{3}\left[\frac{1-\gamma_P^2}{E_P}+\frac{1-\gamma_S^2}{E_S}\right]^{-1} \qquad (8)$$

In this equation, E_P, E_S, γ_P and γ_S represent the Young's modulus of elasticity and Poisson ratio of the particle and substrate, respectively.

Figure 3 shows plots of VDW force for the cases of glass-on-glass and alumina-on-alumina, both in water medium. As can be seen, the VDW force for alumina-on-alumina is larger than that for glass-on-glass which purely originates from the difference in Hamaker constants (see Table 1). It should be mentioned that the increment in the VDW force due to the deformation at the interface is less than 8% for alumina-on-alumina and less than 1% for glass-on-glass (for d ≤ 400 nm).
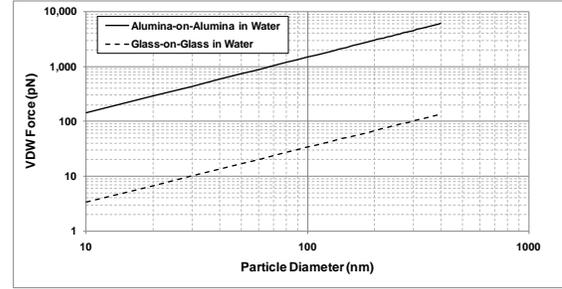

Fig. 3. Plot of VDW force versus particle in water medium.

Ionic double layer (IDL) is a structure that appears near the outer surface of an object when it is placed in a liquid and consists of two parallel layers of ions (see Fig. 4). The first layer is the surface charge (either positive or negative) and the other layer is in the fluid, and electrically screens the first layer. The zeta potential (also known as electrokinetic potential) is used for characterizing of IDL charge. Zeta potential is the potential measured at the slipping plane as shown in Fig. 4. The zeta potential indicates the degree of repulsion/attraction between similarly/oppositely charged objects that are adjacent to each other.

The Zeta potential is a function of the solution pH and the material composition of the particle/substrate (see Fig. 5). Interaction force between a particle and substrate can be attractive or repulsive depending on the zeta potential of particle and substrate. If the particle and the substrate have the same chemical composition, their zeta potentials would be the same regardless of the solution pH. The IDL force is repulsive therefore it does not pose a challenge for particle dislodgement.
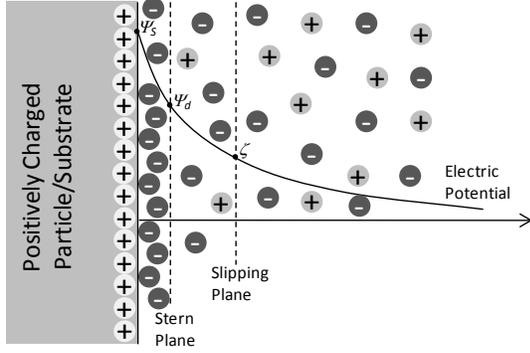
Fig. 4. Schematic of the electric potential variation in a liquid medium in the proximity of a solid object.
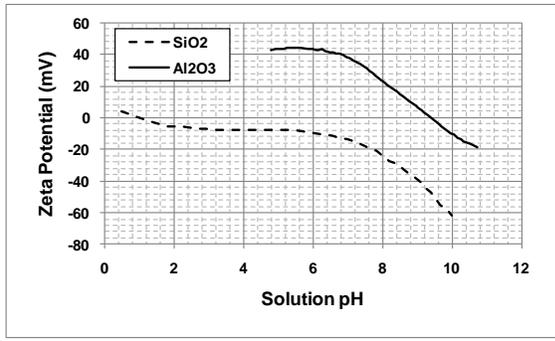

Fig. 5. Plot of zeta potential of alumina and silica as function of solution pH [7].

A particle attached to a substrate in a liquid medium may experience an additional adhesion force if the interface between the particle and substrate is hydrophobic. The hydrophobicity of the interface depends on the average contact angle of the interface as calculated below [8-9]:

$$\cos(\theta_{avg}) = (\cos(\theta_P) + \cos(\theta_S))/2 \qquad (9)$$

In this equation, ϑ_P and ϑ_S represent the contact angle of the particle and substrate, respectively. If the average contact angle (ϑ_{avg}) is larger than 90 degrees, then the interface is hydrophobic and the hydrophobic adhesion force can be calculated using the expression below [9]:

$$F_H = \frac{K_{132}d}{2 z_0^2} \qquad (10)$$

Where K_{132} is the hydrophobic force constant between particle (1) and substrate (2) in the medium (3) and can be calculated as [9]:

$$\log(K_{132}) = -7.0 \times \cos(\theta_{avg}) - 18.0 \qquad (11)$$

For glass and alumina, the contact angles are less than 45 degrees hence the interface between particle and substrate is hydrophilic for glass-on-glass and alumina-on-alumina.

4. Detachment Forces

A USC/MSC system uses a batch of piezoelectric transducers to generate acoustic waves in a tank that is filled by a liquid solution (DI water and a diluted amount of some chemicals). The frequency of the transducers is typically between 150 kHz and 600 kHz for the USC systems and is larger than 600 kHz for the MSC systems. As can be seen in Fig 6, the piezoelectric transducers generate acoustic waves that propagate in the solution, causing the formation of acoustic streaming. Such flow will create a boundary layer when it passes over a substrate surface. The thickness of the acoustic boundary layer can be evaluated as follows [10-11]:

$$\delta = \left(\frac{2\,\nu}{2\,\pi\,f} \right)^{1/2} \qquad (12)$$

In this equation, ν is the kinematic viscosity of the solution and f represents the transducer frequency.
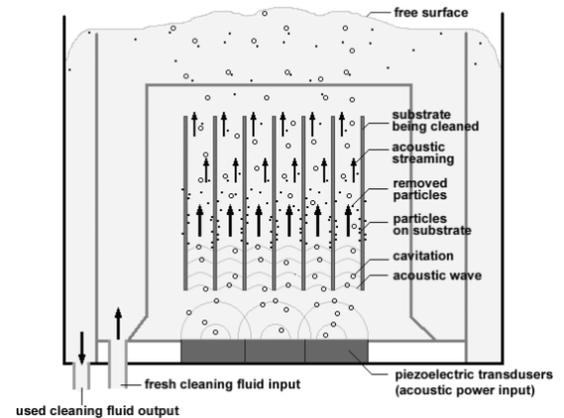

Fig. 6. Schematic of USC/MSC tank and the physical phenomena induced by the piezoelectric transducers [4].

Inspection of equation 12 reveals that the thickness of the acoustic boundary layer can be reduced by either lowering the kinematic viscosity of the solution, for instance by increasing temperature, or increasing the transducer frequency. It should be noticed that lower thickness of acoustic boundary layer allows for exposures of particles to larger flow velocity and consequently increases the chances of particle dislodgment. Figure 7 shows the variation of acoustic boundary layer thickness with the transducer frequency. As can be seen, the thickness of the acoustic boundary layer drops from 640 nm to 430 nm (at 50 C) when the transducer frequency is increased from 430 kHz to 950 kHz.
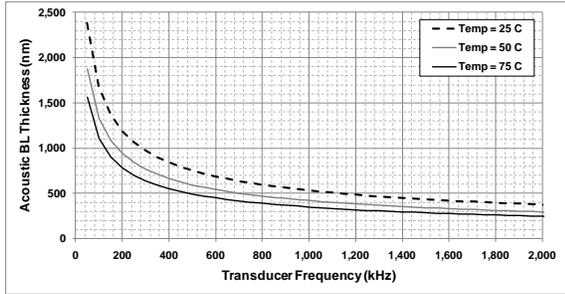

Fig. 7. Plot of acoustic boundary layer thickness versus transducer frequency for various solution temperatures.

The present study focuses on particles smaller than 400 nm that are exposed to transducers with frequencies of 430 kHz and 950 kHz (δ > 400 nm). Therefore, the particle will be within the acoustic boundary layer and exposed to boundary layer flow as shown in Fig. 8. The velocity profile within the boundary layer can be expressed as follows [10-11]:

$$u = u_e \cos(2\pi ft)\left[1 - \exp\left(\frac{-y}{\delta}\right)\cos\left(\frac{-y}{\delta}\right)\right] \quad (13)$$

In this equation t stands time and u_e represents the velocity magnitude outside of the acoustic boundary layer and can be estimated as follows [12]:

$$u_e = \left(\frac{2I}{\rho C}\right)^{1/2} \quad (14)$$

Where I stands for the power intensity of transducer; ρ represents the solution density and C is the speed of the sound in the solution (~ 1475 m/sec).
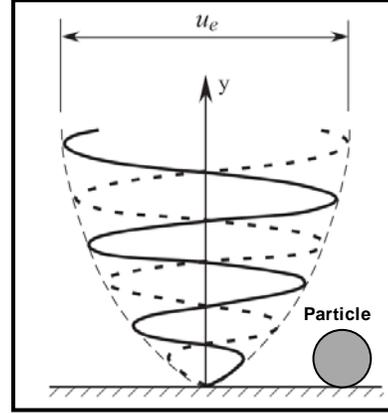

Fig. 8. Schematic of the velocity profile within an acoustic boundary layer that a particle experiences. The sketch shows the velocity profile at two instants separated by one-half period [11].

The aerodynamic drag force (F_D) and moment (M) acting on the particle can be calculated as follows [3-4]:

$$F_D = 1.7 \times (3\pi \mu d V) \quad (15)$$

$$M = 0.370 F_D d \quad (16)$$

In these equations, μ represents the dynamic viscosity of solution and V is the flow velocity at the particle center ($y = d/2$), calculated from eq. 13. The total acoustic streaming force can then be calculated as follows:

$$F_{AS} = F_D + M/(d/2) = 1.74 F_D \quad (17)$$

Figure 9 shows a plot of acoustic streaming force versus particle diameter. As can be seen, the acoustic streaming force increases when the transducer frequency increases, which is due to the reduction in the acoustic boundary layer thickness.
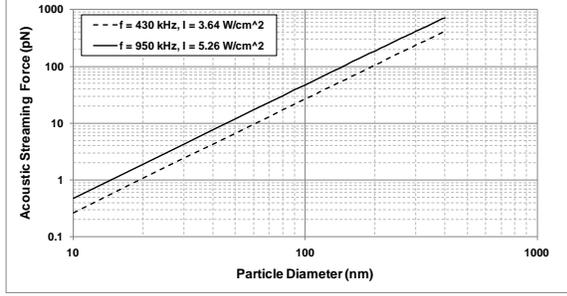
Fig. 9. Plot of acoustic streaming force versus particle diameter for two different transducers: a) a transducer with f = 430 kHz, I = 3.64 W/cm^2; and, b) a transducer with f = 950 kHz, I = 5.26 W/cm^2.

Oscillation of a transducer causes a pressure variation wave that propagates in the solution with the speed of sound. When the pressure variation wave passes over a particle, the particle experiences a force due to the pressure gradient across the particle (see Fig. 10). This force is known as acoustic pressure force and can be calculated by integrating the pressure over the particle surface [13]. Since the wavelength ($\lambda = C / f$) is of the order of 1 mm and is much larger than the diameter of a submicron particle, the pressure gradient can be treated as constant across the particle surface [13]:

$$F_{AP} = \frac{dP}{dx} \times \left(\frac{\pi}{6} d^3 \right) \quad (18)$$

The pressure variation wave is a harmonic wave that can be stated as:

$$P = P_0 \sin\left(\frac{2\pi x}{\lambda} \right) = P_0 \sin\left(\frac{2\pi f x}{C} \right) \quad (19)$$

In this equation, P_0 is the amplitude of pressure variation wave and can be described as [12]:
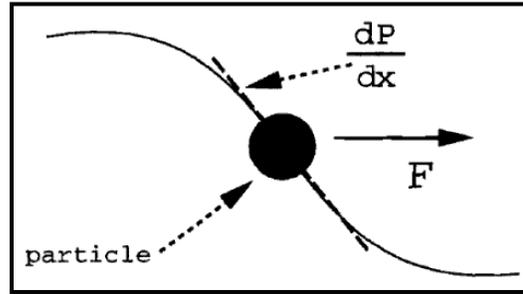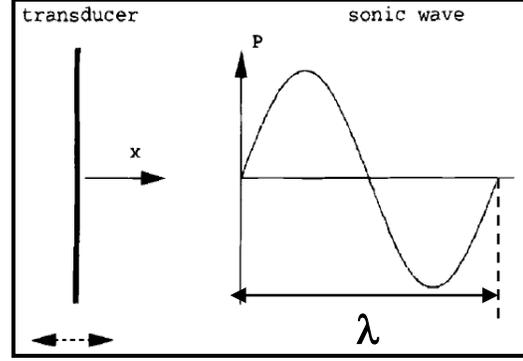
$$P_0 = \sqrt{2 \rho I C} \quad (20)$$

Fig. 10. Schematic of a pressure variation wave induced by an oscillating transducer (top) and the pressure gradient across a particle (bottom) [13].

By substituting eq. 19 and 20 into eq. 18, one can obtain an expression for the maximum acoustic pressure force that a particle can experience:

$$F_{AP} = 2\pi f \left(\frac{\pi}{6} d^3 \right) \sqrt{\frac{2\rho I}{C}} \quad (21)$$

Figure 11 illustrates the variation of acoustic pressure versus the particle diameter. Inspection of this figure reveals that acoustic pressure force: a) increases by increasing the particle diameter and transducer frequency; and, b) is more than one order of magnitude smaller than the acoustic streaming force.
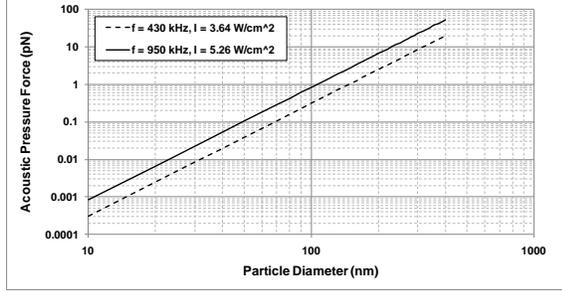
Fig. 11. Plot of acoustic pressure force versus particle diameter for two different transducers: a) a transducer with f = 430 kHz, I = 3.64 W/cm^2; and, b) a transducer with f = 950 kHz, I = 5.26 W/cm^2.

The pressure variation wave causes high and low pressure in the solution as shown in Fig. 10. The low pressure half-cycle can cause expansion of pre-existing bubbles and, potentially, formation of new bubbles. The high pressure half cycle can cause compression or, potentially, implosion of bubbles. To this end, two classes of acoustic cavitations are defined: a) steady cavitation that is a process in which bubbles oscillates in size and shape; and, b) transient cavitation in which bubbles implodes producing a shock wave. In a USC/MSC, the steady cavitation is the desired type of cavitation and will be the focus of the present study.

For a bubble of diameter d_B, the natural frequency is given by Minnaert formula [14]:

$$f = \frac{1}{\pi d_B}\left[\frac{3k}{\rho}\left(P_0 + \frac{4\sigma}{d_B}\right) - \frac{4\sigma}{\rho d_B}\right]^{1/2} \qquad (22)$$

In this equation, P_0 (=101.325 kPa) is the atmospheric pressure, k is the polytropic gas constant ($1 \leq k \leq 1.4$) and σ is the surface tension of the solution. For a given transducer frequency, the active bubbles are the ones that resonate when exposed to ultrasound waves. In other ones, active bubbles are the ones that have a natural frequency equal to the transducer frequency. Figure 12 shows a plot of active bubble diameter. As can be seen, the active bubble size drops from 16 µm to 8 µm when the transducer frequency increases from

430 kHz to 950 kHz. It should be noticed that those bubbles are more than one order of magnitude larger than the particle sizes studied herein ($d \leq 400$ nm).
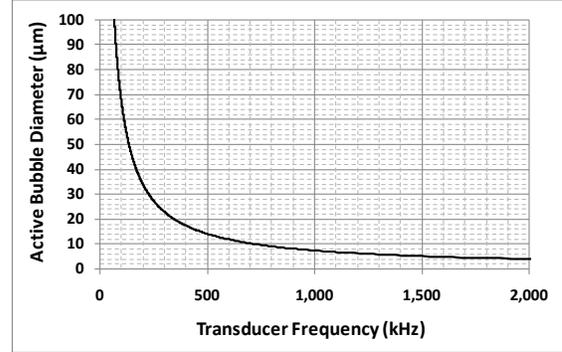

Fig. 12. Plot of active bubble diameter versus transducer frequency.

The detachment force applied on a particle due to radial oscillation of steady bubble (acoustic cavitation force) can be estimated as follows [2]:

$$F_{AC} \approx \frac{\pi}{6}\rho \omega^2 d^3 d_B \left(\frac{R_B}{r}\right)^5 \qquad (23)$$

In this equation, ω (=$2\pi f$) is the angular frequency; R_B (= d_B / 2) is the radius of active bubble corresponding to the transducer frequency f and r is the distance between the bubble center and the particle surface, as illustrated in Fig. 13. Inspection of eq. 23 reveals that the acoustic cavitation force declines with the fifth power of distance between bubble center and particle (r). Hence, the maximum acoustic cavitation force occurs when the oscillating bubble comes into contact with the particle (i.e. R_B/r = 1).
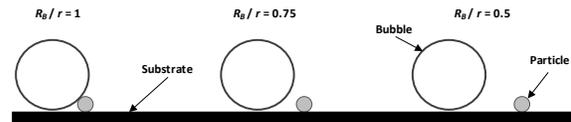

Fig. 13. Schematic of position of a bubble relative to a particle for three different R_B / r values.

Figure 14 shows the plot of acoustic cavitation versus particle diameter for R_B/r = 1. As can be seen, acoustic cavitation force increases by

increasing the transducer frequency. It can be also observed that the acoustic cavitation force is about two orders of magnitude larger than the acoustic pressure force.
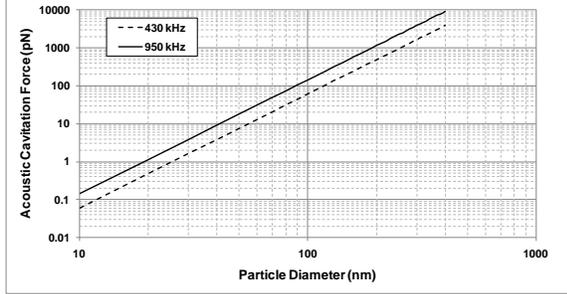

Fig. 14. Plot of acoustic cavitation force versus particle diameter for two different transducers frequencies: 430 kHz and 950 kHz.

5. Particle Dislodgement Inspection

In this section, the detachment of glass/alumina particles from glass/alumina substrates is investigated. As mentioned in section 2, rolling dislodgment is the most likely method of dislodgment for a particle. Hence, a scaling factor is introduced to scale the adhesion force (in this case, the VDW force) as follows:

$$F_{VDW}^* = F_{VDW} \times \left(\frac{a}{d/2 - b} \right) \qquad (24)$$

Where $a / (d/2 - b)$ is the scaling factor that originates from eq. 1 and is smaller than 0.05 for both glass and alumina particles (10 nm ≤ d ≤ 400 nm). Rolling dislodgement occurs if the detachment force exceeds the scaled VDW forced expressed in eq. 24.

Figure 15 illustrates plots of detachment forces and the scaled VDW forces versus particle diameter. Inspection of Fig. 15 reveals that: a) for the case of alumina-on-alumina, particles larger than 50 nm can be dislodged; b) for the case of glass-on-glass, particles larger than 10 nm can be dislodged; and, c) the dominant detachment force is acoustic cavitation force for particles larger than 35 nm (for f = 950 kHz) and 43 nm (for f = 430 kHz).
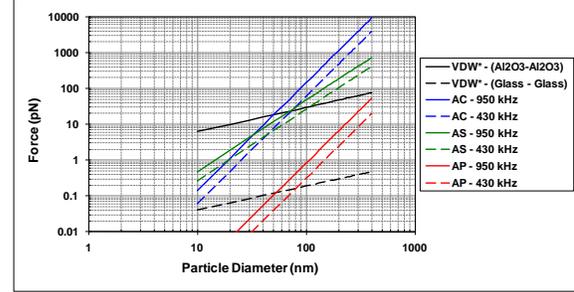

Fig. 15. Plot of detachment forces and scaled VDW forces for the cases of alumina-on-alumina and glass-on-glass.

6. Conclusions

The adhesion and detachment of spherical particles with diameter less than 400 nm was investigated for the cases of glass-on-glass and alumina-on-alumina as a substitute for a more general approach. It was found that the VDW force is the dominant force of adhesion that needs to be overcome by detachment forces induced by transducers in a USC/MSC tank. The acoustic pressure force appeared to be much smaller than the acoustic streaming and acoustic cavitation forces. It was also found that the dominant detachment force is acoustic cavitation force for particles larger than 35 nm (for f = 950 kHz) and 43 nm (for f = 430 kHz).

Inspection of the adhesion and detachment forces revealed that the detachment threshold limit is 50 nm for alumina particles whereas glass particles as small as 10 nm can be successfully dislodged. It should be mentioned that the analysis conducted herein is based on the assumption that the acoustic waves are not blocked by any structure to cause shadowing effect. If shadowing is an obstacle for substrate cleaning then the structures supporting the substrate need to be redesigned to allow for the substrate surface to be uniformly exposed to the acoustic waves.

References

1. Vereecke, G., Parton, E., Holsteyns, F., Xu, K., Vos, R., Mertens, P.W., Schmidt, M. O., Bauer, T., Siltronic, W., "Investigating the role of gas cavitation in megasonic nanoparticle Removal," Micromagazine.com Article.

2. Kim, W., Kim,T. H., Choi, J. and Kim, H. Y. "Mechanism of particle removal by megasonic waves," Appl. Phys. Lett., vol. 94, 081908, 2009.

3. C. Toscano, G. Ahmadi, "Particle removal Mechanisms in Cryogenic surface cleaning," Journal of Adhesion, vol. 79, pp. 175-201, 2003.

4. Busnaina, A., "Nanomanufacturing Handbook," CRC Press, First Edition, 2006.

5. Johnson, K., Kendall, K. and Roberts, A. D., "Surface Energy and Contact of Elastic Solids," Proc. R. Soc., London, 324, pp. 301-313, 1971.

6. Zhang, F., Busnaina, A. A., Fury, M. A., Wang, S. Q, "The Removal of Deformed Submicron Particles from Silicon Wafers by Spin Rinse and Megasonics," Journal Of Electronic Materials, (2000).

7. Brunelle, J. P., "Preparation of Catalysts by Metalic Complex Adsorption on Mineral Oxides," Pure & Appi. Chern., Vol. 50, pp. 1211—1229.

8. Birdi, K.S., "Handbook of Surface and Colloid Chemistry," CRC Press, Third Edition, 2009.

9. Yoon, R.H., Flinn, D. H. and Rabinovich, Y. I., "Hydrophobic Interactions between Dissimilar Surfaces," Journal of Colloid and interface Science, vol. 185, 363–370 (1997).

10. Schlichting, H. and Gersten, K., "Boundary Layer Theory," Springer Publication, 8th Edition, 2000.

11. Culick, F. E. and Kuentzmann, P., "Unsteady Motions in Combustion Chambers for Propulsion Systems," NATO Research and Technology Organization, Originator's Reference # RTO-AG-AVT-039 AC/323(AVT-039)TP/103.

12. Keswani, M. , Raghavan, S., Deymier, P. and Verhaverbeke, S. "Megasonic cleaning of wafers in electrolyte solutions: Possible role of electro-acoustic and cavitation effects," Microelec. Eng., vol. 86, pp. 132-139, 2009.

13. Olim, M. "A theoretical evaluation of megasonic cleaning for submicron particles," J. Electrochem. Soc., vol. 144, no. 10, pp. 3657-3659, 1997.

14. Edmonds, P. D., "Methods of Experimental Physics," Volume 19, Ultrasonics, Academic Press, 1981.